Contrib Mineral Petrol (1984) 87:376–387

Contributions to Mineralogy and Petrology

Geochemical relationships between anorthosite and associated iron-rich rocks, Laramie Range, Wyoming

S.A. Goldberg
Department of Geology, University of North Carolina, Chapel Hill, NC 27514, USA

Abstract. Rocks enriched in iron oxide and mafic silicates are commonly present as minor volumes of Proterozoic anorthosite complexes. In the Laramie Range, Wyoming, anorthositic rocks, gabbros, and iron oxide ore have been chemically analyzed to determine if the spatial association is a result of genetic relationships between the rock types.

Variations in abundances of REE, Th, Sc, and Sr in whole-rock and in mineral separates from anorthositic rocks provide evidence for the presence of trapped intercumulus liquid. Initial $^{87}Sr/^{86}Sr$ ratios in apatites separated from iron oxide ore (0.70535 ± 0.00004) are analogous to initial $^{87}Sr/^{86}Sr$ ratios in Laramie Range anorthosite (0.70531 and 0.70537). In addition, REE abundances in calculated parental liquids for both anorthositic rocks and iron ore are similar, providing further evidence for a comagmatic relationship.

Trace element and textural characteristics of spatially associated Laramie Range gabbros indicate that they are not mixtures of the trapped liquid and cumulus components which formed anorthositic rocks. It is suggested that gabbros are early differentiation products of a high-Al gabbroic magma which subsequently crystallized large volumes of plagioclase to produce the anorthosite massif.

Introduction

Iron oxide-rich dikes and lenses are typically associated with Proterozoic anorthosite massifs. Although the spatial association of Fe–Ti oxide ore and anorthosite has been recognized for more than a century, a genetic relationship between the two has not been clearly established. A sizable amount of petrological data suggests that massif-type anorthosites are magmatic in origin, perhaps derived from a leucogabbroic (e.g. Simmons and Hanson 1978; Wiebe 1980) or high-Al basaltic magma (Emslie 1978). The close association of anorthosite and oxide ore suggests a related origin.

Hypotheses for the origin of Fe–Ti oxide deposits associated with anorthosite include hydrothermal replacement (Ross 1941), metamorphic migration (Ramberg 1948; Hagner 1968), residual liquid segregation (Bateman 1951; Lister 1966; Roelandts and Duchesne 1979) and liquid immiscibility (Philpotts 1967, 1981). The ability to distinguish among the various hypotheses requires an understanding of the magmatic processes responsible for the formation of anorthosite.

There is evidence to suggest that anorthositic parental magmas differentiated to form minor volumes of oxide-rich rock. For example, mafic and oxide-rich dikes and segregations from the Marcy massif of the Adirondacks are interpreted as late-stage differentiates of a melt which crystallized anorthosite. This interpretation is based on evidence from field relations, mafic-silicate mineral compositions, and complementary REE patterns (Ashwal and Seifert 1980; Ashwal 1982). Orthopyroxene-bearing monzonitic and granitic rocks are also spatially associated with Proterozoic anorthosites. However, field evidence and geochemical relations (e.g. Seifert 1978; Fountain et al. 1981) indicate that monzonitic and granitic rocks are not comagmatic with anorthosite.

Anorthositic rocks from the southern part of the Laramie Range, Wyoming, have been chemically analyzed in order to formulate a model for their crystallization history. Associated gabbros and iron oxide dikes have also been analyzed in order to determine if they are genetically related to anorthosite.

Geological relations

The Laramie anorthosite complex was emplaced into lower Proterozoic terrain consisting of deformed metaigneous and metasedimentary rocks (Hills and Houston 1979). The complex consists of anorthosite, gabbroic anorthosite, anorthositic gabbro, olivine-rich anorthositic rocks, and associated gabbro, magnetite ore, and monzonite (Fig. 1). Although cataclastic deformation features are apparent, cumulus textures are preserved in anorthositic rocks. Cumulus and intercumulus minerals consist mainly of plagioclase, augite, olivine, and titaniferous magnetite. Minor inverted pigeonite, amphibole, biotite, potassium feldspar, and apatite are also observed.

Field relationships have been described by Fowler (1930), Diemer (1941), Newhouse and Hagner (1957), Klugman (1966), and Smithson and Hodge (1972). Klugman inferred relative ages for various rocks of the complex. In order of increasing age, these are monzonite, gabbro, gabbroic anorthosite, and anorthosite. Gravity data (Hodge et al. 1973) indicate that the Laramie anorthosite mass is 4 km thick and that it is not underlain by higher density mafic rocks.

Geochronological investigations suggest a minimum age for Laramie anorthosite of approximately 1,450 m.y. Rocks showing intrusive relationships to anorthosite include mon-

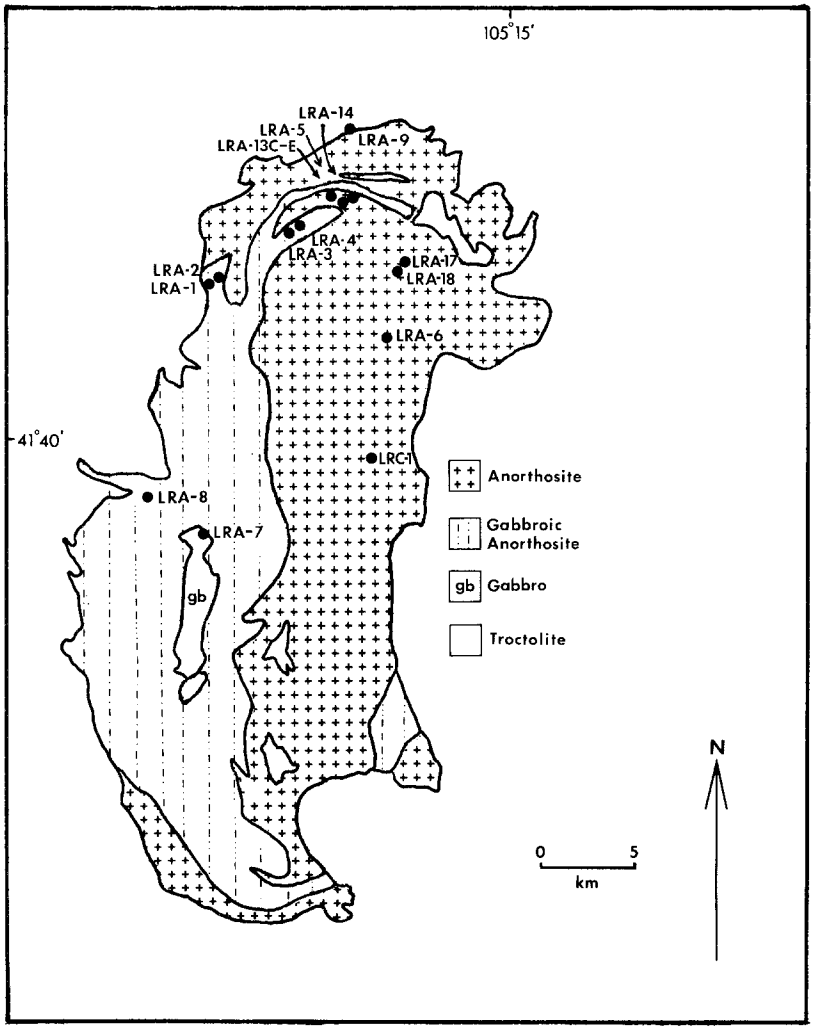

Fig. 1. Simplified geological map of anorthositic rocks from the Laramie Range, Wyoming (after Klugman 1966; Hagner 1968)

zonite and Sherman granite (Fowler 1930; Klugman 1966). Rb–Sr and $^{207}Pb/^{206}Pb$ isotopic data for the Sherman granite indicate crystallization ages of $1{,}430 \pm 20$ m.y. and $1{,}420 \pm 20$ m.y., respectively. Similar $^{207}Pb/^{206}$ ages of $1{,}432 \pm 15$ m.y. and $1{,}424 \pm 15$ m.y. were obtained for samples of monzonite (Subburayudu et al. 1975). Rb–Sr isotopic data for monzonites yield ages of 1,350 m.y. (Fenton and Faure 1969), 1,290 m.y., and 1,950 m.y. (Subburayudu et al. 1975). This latter age is based on an isochron which presumably reflects the incorporation of older country rock. In addition to these studies, Hills and Armstrong (1974) reported K–Ar ages for hornblende and biotite in a sample of Laramie Range anorthosite collected in a magnetite deposit. The hornblende yielded an apparent age of 1,500 m.y. and the biotite, 1,390 m.y.

Analytical methods

Whole-rock major element compositions were determined by X-ray fluorescence (XRF) spectrometry, using a fused disk technique similar to that of Norrish and Hutton (1969). Abundances of Ni, Rb, Sr, and Zr were also determined by XRF, using pressed powder disks as described by Norrish and Chappell (1967). Abundances of Na, Fe, and Sc, Cr, Co, Cs, Ba, La, Ce, Nd, Sm, Eu, Tb, Yb, Lu, Hf, Ta, Th, and U were determined by instrumental neutron activation analysis (INAA) using modified procedures of Gordon et al. (1968) and Goles (1977). H_2O^+ contents of powdered whole-rock samples were determined with a moisture analyzer utilizing an electrolytic cell.

Mineral compositions were determined by wavelength-dispersive electron microprobe analysis using the data reduction method of Bence and Albee (1968) with alpha factors of Albee and Ray (1970). Operating conditions were 15 kv accelerating potential and 15 na sample current. U.S.G.S. standard rocks were used as primary standards for XRF, INAA, and H_2O^+ analyses. Natural and synthetic standards were used in electron microprobe analysis. Facilities for XRF, INAA, and electron microprobe analysis were provided by the University of Oregon.

Strontium isotopic analyses were determined with a 30 cm radius, 90° magnetic sector, triple filament thermal ionization mass spectrometer at the University of North Carolina at Chapel Hill. Strontium isotopic compositions were measured on unspiked samples prepared using standard ion exchange techniques. Isotopic ratios have been normalized to a $^{86}Sr/^{88}Sr$ ratio of 0.1194. Recent analysis of Eimer and Amend strontium carbonate yields a ratio of 0.70801 ± 0.00008.

Chemical variations in whole-rock samples

Samples of anorthositic rock collected for analysis contain cumulus plagioclase and interstitial mafic phases consisting of anhedral pyroxene, olivine, and iron oxide. Major and trace element analyses of whole-rock samples are presented in Tables 1–3. Relative enrichments of compatible and in-

compatible elements are used to identify fractionation processes. Sr, a plagioclase-compatible element, is enriched relative to the plagioclase-incompatible elements Th and La. Figure 2 shows Sr to be inversely correlated with both Th and La. Thorium is a highly excluded element in the observed mineral phases and will preferentially remain in a residual liquid during crystal fractionation. In contrast, the concentration of Sr is directly proportional to modal plagioclase. The relative concentration of Th is therefore almost entirely a function of the amount of trapped liquid present in a cumulate rock. Although the K_d value for La between plagioclase and liquid (0.12 to 0.24, Drake and Weill 1975) is probably higher than that of Th, La will nevertheless preferentially concentrate in a residual liquid. As in the case of Th, the inverse correlation between La and Sr (Fig. 2) and thus between La and modal plagioclase necessitates the presence of a trapped liquid component.

Those anorthositic rocks which are mixtures of cumulus plagioclase and trapped liquid can also be identified on a plot of La versus Sc, as shown by Salpas et al. (1983). Rocks with the largest trapped liquid component should contain the largest amount of orthocumulus pyroxene and the largest incompatible element abundances. As clinopyroxene preferentially incorporates Sc, a plot of La versus Sc should produce a positive trend, which is observed for Laramie Range anorthositic rocks (Fig. 3).

Rare earth element data for Laramie anorthositic rocks are listed in Table 1. The rocks are all light REE enriched ($La_N/Sm_N = 2.1$ to 6.3), and are characterized by positive Eu anomalies (Fig. 4). In general, an increase in trivalent REE is observed with increasing amounts of mafic minerals. Similar features have been observed in other Proterozoic anorthosite massifs (Simmons and Hanson 1978; Ashwal and Seifert 1980; Demaiffe and Hertogen 1981), and are consistent with the accumulation of large volumes of plagioclase and the entrapment of varying amounts of liquid.

REE data for rocks sampled from magnetite ore deposits (Table 3) exhibit light REE enrichment ($La_N/Sm_N = 1.7$ to 1.9), negative Eu anomalies (Fig. 5), and La contents as large as 635 times chondrites. The total REE abundances in these ores are proportional to modal apatite, and can be interpreted in terms of either cumulus processes or late-stage magmatic differentiation.

Samples of gabbro (LRA-7, LRA-9) and ferrogabbro (LRA-16) (Fig. 6) differ from anorthositic rocks and iron-rich ore in their REE characteristics. Gabbroic rocks (Table 2) have significantly less fractionated REE patterns characterized by relatively low La_N/Sm_N ratios of 1.0 to 1.3, compared to values of 2.1 to 6.2 for plagioclase-rich rocks, and 1.7 to 1.9 for iron-rich ore. Although sample LRA-16 exhibits a large negative Eu anomaly and contains large total REE abundances (Fig. 6), it differs from ore samples by its flat light REE pattern.

REE data are also presented as a plot of La_N/Sm_N versus Lu_N in Fig. 7. Samples of gabbro are clearly distinguished by their low La_N/Sm_N ratios, and form a distinct trend (C). Samples of gabbroic anorthosite and magnetite ore form trend (B) with a shallow slope, connected to a steeper trend (A) which contains only anorthosite. Anorthositic rocks in trends (A) and (B) represent mixtures of cumulus plagioclase and trapped liquid. Samples of iron ore in trend (B) apparently crystallized from trapped liquid enriched in the components of iron oxide and apatite. As modal apatite is a significnat phase only in trends (B) and (C), the change in slope between (A) and (B) and the progressive decrease in La_N/Sm_N with Lu_N reflect the presence of this mineral.

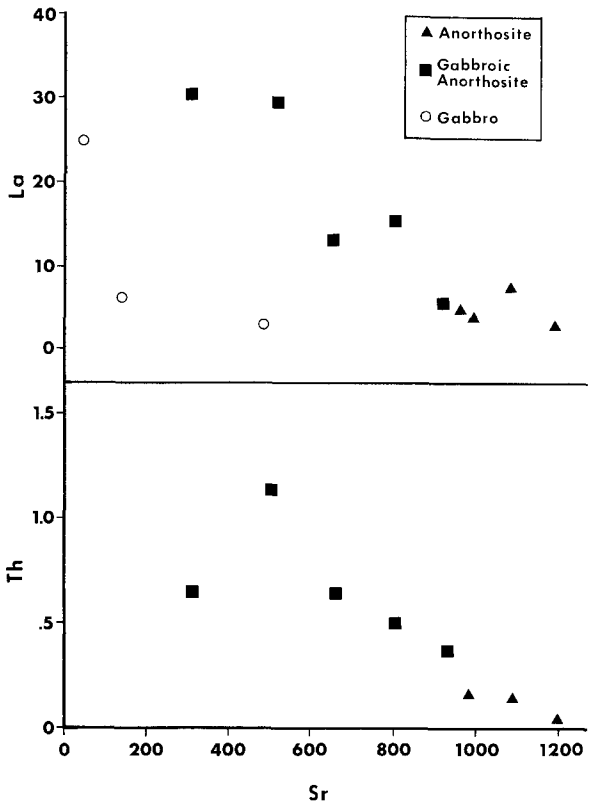

Fig. 2. Plot of ppm Th versus ppm Sr and ppm La versus ppm Sr for Laramie Range anorthosite, gabbroic anorthosite, and gabbro

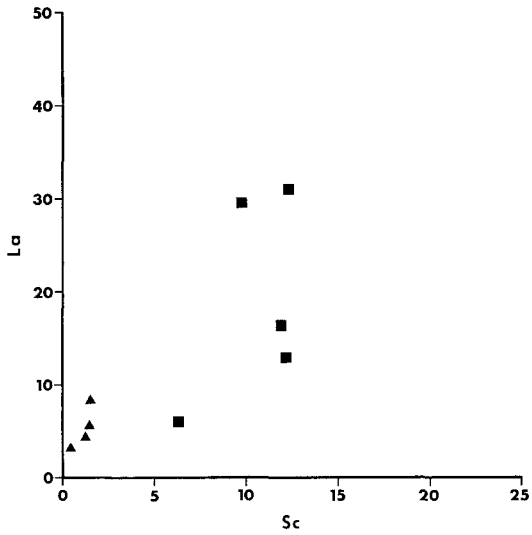

Fig. 3. Plot of ppm La versus ppm Sc for Laramie Range anorthosite and gabbroic anorthosite. Samples are labelled as in Fig. 2

Compositional variations in mineral phases

Because cumulate rocks can be compositionally far removed from their parental liquids, whole-rock analyses may

Table 1. Major and trace element abundances for Laramie Range anorthositic rocks. Whole-rock samples are labelled as anorthosite (A), gabbroic anorthosite (GA), and iron oxide-rich gabbroic anorthosite (MtGA)

	LRA1	LRA2	LRA3	LRA4	LRA5	LRA8	LRA13C	LRA13D	LRA13E
	GA	GA	A	A	A	GA	MtGA	A	GA
SiO_2	50.39	58.54	54.84	55.23	51.85	50.73	43.54	51.13	50.11
TiO_2	1.74	0.67	0.09	0.07	0.33	1.58	1.51	0.05	0.26
Al_2O_3	22.06	18.35	26.53	25.91	28.01	21.96	13.92	28.05	24.23
FeO	7.18	6.75	1.39	1.13	2.11	7.06	19.80	1.58	5.74
MnO	0.10	0.13	0.01	0.01	0.04	0.09	0.25	0.02	0.06
MgO	2.55	0.79	0.82	0.93	0.65	2.79	6.93	1.43	3.66
CaO	9.72	3.62	8.87	9.03	10.53	9.38	7.67	11.49	10.19
Na_2O	4.19	4.41	5.08	5.01	3.94	3.79	2.48	3.88	3.45
K_2O	0.80	5.38	1.04	1.10	1.11	0.88	0.71	0.54	0.76
P_2O_5	0.21	0.18	0.04	0.05	0.55	0.30	1.48	0.01	0.05
H_2O^+	0.52	0.37	0.45	0.60	0.49	0.49	0.62	1.17	1.11
Total	99.46	99.19	99.16	99.07	99.61	99.05	98.91	99.35	99.62
Fe	5.34	5.62	1.12	0.90	1.64	5.27	14.60	1.29	4.46
Sc	11.87	12.29	1.35	1.37	1.54	12.22	9.77	0.53	6.50
Cr	15.6	5.5	3.4		6.9	22.7	16.2	1.1	39.7
Co	17.4	3.39	2.52	2.36	7.69	19.3	71.3	6.92	25.5
Ni		40.0				132.0	46.0	12.0	
Ta	0.66	1.28			0.06	0.37			
Hf	1.45	22.1	0.20		0.19	1.54			0.50
Zr	64.0	893.0	21.0	16.0	<10.0	66.0	78.0	<10.0	27.0
Th	0.49	0.61	0.15		0.14	0.64	1.13	0.04	0.36
Na	3.11	3.27	3.77	3.72	2.92	2.81	1.84	2.90	2.56
Rb	6.0	60.0	7.0	11.0	4.48*	8.0	13.0	2.18*	23.0
Sr	801.0	303.0	978.0	972.0	1087.0	653.0	507.0	1195.0	930.0
Cs		0.52		0.18					1.28
Ba	683.0	2640.0	557.0	478.0	428.0	525.0	322.0	329.0	279.0
La	16.2	31.2	4.55	5.0	8.3	12.6	29.9	3.5	5.62
Ce	36.3	64.6	7.8	8.2	17.7	26.2	51.9	5.95	12.21
Nd	18.9							2.2	
Sm	4.30	8.98	0.60	0.99	2.25	3.17	7.03	0.34	1.48
Eu	2.90	6.38	2.20	1.87	1.68	2.40	2.05	1.05	1.08
Tb	0.64	1.19			0.24	0.43	1.01		0.25
Yb	1.29	3.45		0.21	0.37	0.88	2.07		0.57
Lu	0.157	0.501	0.016	0.026	0.053	0.132	0.284		0.073

Oxides, Fe, and Na in wt.%; remainder of data in ppm

* Analysis by isotope dilution mass spectrometry

not reflect parental liquid compositions. However, major and trace element variations in solid solution mineral phases (Tables 4 and 5) can be used to document magmatic differentiation. Variations in the MgO/MgO + FeO ratio of mafic minerals and in the An content of coexisting plagioclase in cumulate rocks have been used to infer fractional crystallization and cumulus processes within a parental magma (e.g. Raedeke and McCallum 1980; Longhi 1982). The variation of trace and major element data in plagioclase mineral separates can also reveal compositional trends indicative of cumulus processes. In Fig. 8, ppm Sm is plotted against MgO/MgO + FeO, ppm Th, and mole % An for plagioclase from five different anorthositic rocks. Both Sm and Th are enriched in plagioclase with the lowest MgO/MgO + FeO and mole % An values. Although these data are consistent with the crystallization of plagioclase from an evolving parental liquid, large variations in trace element abundances (Table 4) require excessive amounts of fractionation. The observed five-fold enrichment in Sm could be explained by 81% plagioclase crystallization from a parental magma, but this amount is considered to be improbable for all but the most feldspathic magmas.

REE data for plagioclase mineral separates from Laramie Range anorthositic rocks are presented graphically in Fig. 9. The patterns are characteristically light REE enriched, with large positive Eu anomalies. Plagioclase REE data from other anorthosite bodies (Griffin et al. 1974; Roelandts and Duchesne 1979; Ashwal and Seifert 1980) show similar patterns with slight differences attributed to different crystallization histories. Plagioclase mineral separates from Laramie anorthositic rocks show a three-fold variation in total REE abundances. This large range in trace element content is interpreted to result from post-cumulus growth from a trapped liquid. In the presence of trapped liquid, cumulus plagioclase would be expected to grow and acquire greater amounts of incompatible elements as the trapped liquid solidifies. Plagioclase mineral separates with the largest concentrations of incompatible elements are thus interpreted to have equilibrated with the largest quantity of trapped liquid, whereas those with smaller concentra-

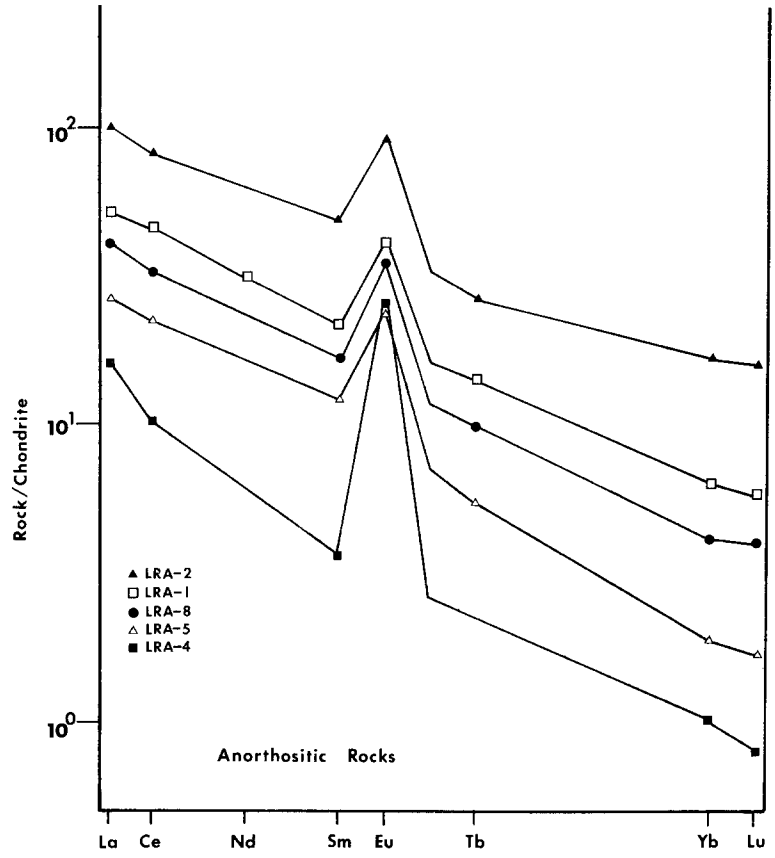

Fig. 4. REE plots for representative samples of Laramie Range anorthositic rock

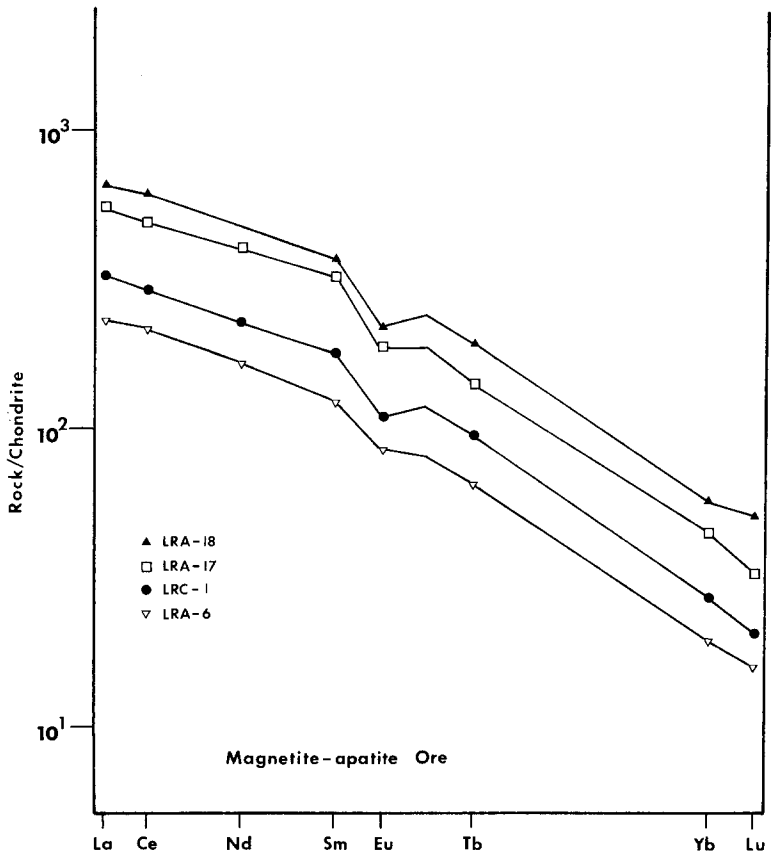

Fig. 5. REE plots of Laramie Range magnetite-apatite ore

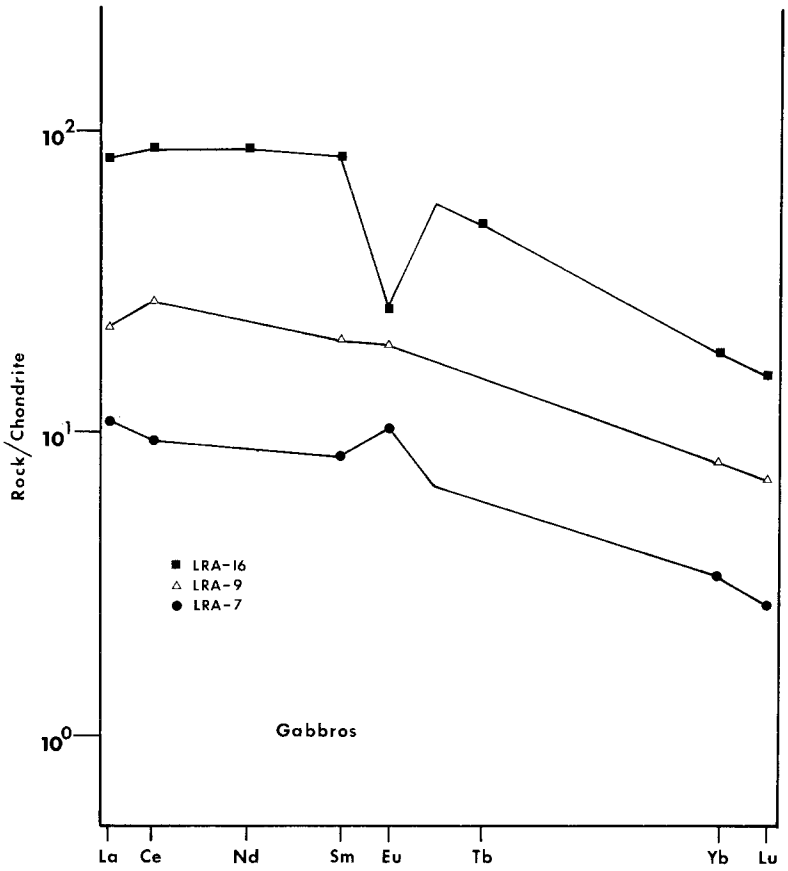

Fig. 6. REE plots of Laramie Range gabbros

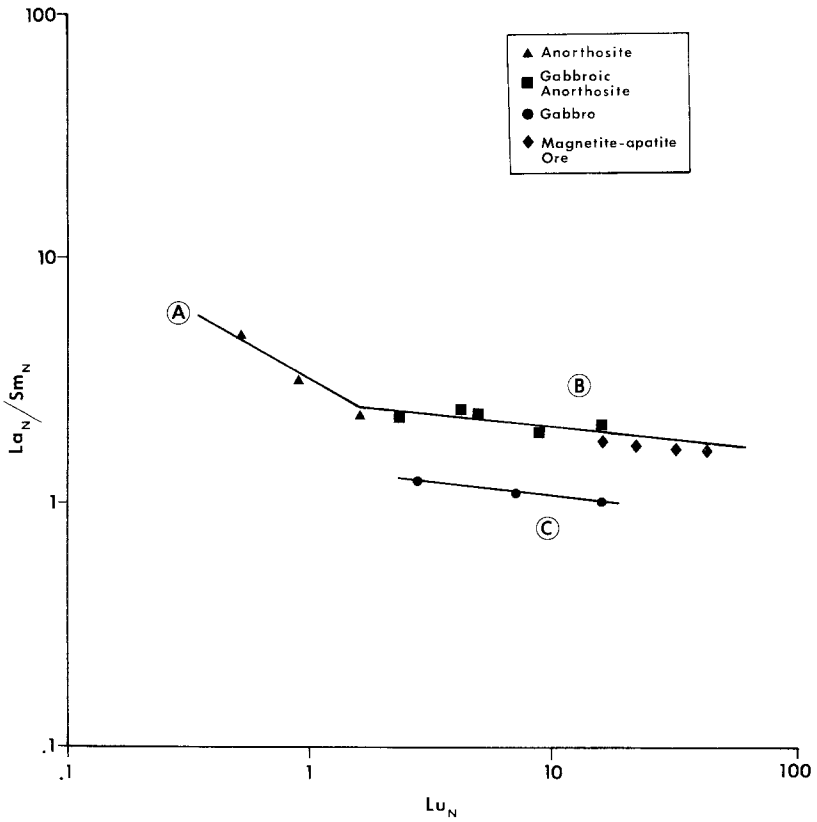

Fig. 7. Plot of La_N/Sm_N versus Lu_N for Laramie Range anorthosite (A), gabbroic anorthosite and magnetite ore (B), and gabbro (C)

Table 2. Major and trace element abundances for Laramie Range gabbros

	LRA7	LRA9	LRA16
SiO_2	47.18	45.17	31.18
TiO_2	1.38	1.87	5.63
Al_2O_3	15.40	12.54	2.08
FeO	10.60	14.47	42.69
MnO	0.15	0.23	0.67
MgO	10.90	8.68	3.33
CaO	11.64	11.14	9.45
Na_2O	2.37	2.63	0.12
K_2O	0.31	0.38	0.07
P_2O_5	0.23	0.22	1.90
H_2O^+	0.72	1.18	1.00
Total	100.88	98.51	98.12
Fe	8.24	11.25	34.30
Sc	26.2	32.2	76.2
Cr	50.0	579.0	52.0
Co	46.3	76.6	21.8
Ni	20.0		<10.0
Ta	0.08		0.81
Hf	0.88	2.07	5.90
Zr	29.0	76.0	210.0
Na	1.76	1.95	0.09
Rb	<5.0	<5.0	7.0
Sr	487.0	129.0	47.0
Ba	194.0		
La	3.37	7.01	25.8
Ce	7.6	21.7	71.2
Nd			51.0
Sm	1.61	3.88	15.7
Eu	0.76	1.40	1.84
Tb			2.18
Yb	0.68	1.67	3.92
Lu	0.088	0.226	0.51

Oxides, Fe, and Na in wt.%; remainder of data in ppm

Table 3. Major and trace element abundances for Laramie Range iron ore

	LRA6	LRA17	LRA18	LRC1
SiO_2	0.79		0.50	
TiO_2	16.86		14.96	
Al_2O_3	3.24		2.47	
Fe_2O_3	43.40		6.07	
FeO	14.01		38.17	
MnO	0.28		0.23	
MgO	0.86		0.82	
CaO	11.54		21.49	
Na_2O	0.02		0.06	
K_2O	0.00		0.00	
P_2O_5	7.08		13.33	
H_2O^+	1.19		0.11	
Total	99.27		98.21	
Fe	35.3	19.1	22.7	31.7
Sc	13.71	9.69	12.34	12.93
Cr	827.0	197.0	299.0	6.9
Co	90.5	63.9	68.1	81.8
Ta	0.96	0.61	1.47	
Hf	1.84	1.48	2.36	1.88
Zr	71.0		92.0	
Th	0.79	3.23	2.34	1.51
Na	0.02	0.04	0.05	0.02
Rb	<5.0	<5.0	<5.0	<5.0
Sr	147.0		304.0	
La	71.8	172.0	200.0	99.0
Ce	170.0	396.0	479.0	233.0
Nd	98.0	235.0		136.0
Sm	23.6	60.6	70.0	33.9
Eu	6.0	13.5	14.8	7.9
Tb	2.9	8.6	8.9	4.3
Yb	4.1	9.3	12.1	5.7
Lu	0.50	1.03	1.36	0.68

Oxides, Fe, and Na in wt.%; remainder of data in ppm

tions equilibrated with proportionally smaller quantities of trapped liquid. Only those plagioclase separates with the lowest incompatible element abundances can be explained as primary cumulus phases.

Sr isotopic data

Apatite is a common mineral in many iron ore deposits, and may constitute as much as one-third the total volume of a deposit. Because apatite incorporates negligible amounts of Rb, its Sr isotopic composition should be indicative of an initial $^{87}Sr/^{86}Sr$ ratio. Similarly, $^{87}Sr/^{86}Sr$ ratios from samples of Rb-poor anorthosite should also approximate initial Sr ratios. In order to test these assumptions, two samples of apatite were analyzed for Rb concentration by isotope dilution mass spectrometry. Apatite from ore sample LRA6 contains 0.09 ppm Rb and from sample LRA18, 0.14 ppm. These Rb abundances are very low relative to Sr (>400 ppm), and preclude any significant change in the initial $^{87}Sr/^{86}Sr$ ratio of apatite over the last 1.45 b.y., an estimated age for Laramie anorthosite.

Two whole-rock samples of anorthosite were also analyzed for both Rb concentration and Sr isotopic composition. Measured $^{87}Sr/^{86}Sr$ ratios in anorthosite samples LRA5 and LRA13D are 0.70560 and 0.70548 (Table 6). Abundances of Rb in the two anorthosites are 4.48 and 2.18 ppm (Table 1). Assuming an age for Laramie anorthosite of 1.45 b.y., calculated initial ratios are 0.70531 and 0.70537. These initial ratios from anorthosite are similar to those obtained by Heath and Fairbairn (1969) on Laramie Range anorthosite, and are in agreement with Sr isotopic data from four samples of apatite (Table 6) which yield an average $^{87}Sr/^{86}Sr$ ratio of 0.70535 ± 0.00004. It is noted that an initial ratio from anorthosite of 0.7028 has been reported by Subbarayudu et al. (1975). The similarity in the Sr initial ratios from the two rock types as determined in this study suggests that magnetite ore can be derived from the same source, or the same parental magma as anorthosite.

Petrogenetic relationships

Anorthosite

Anorthositic rocks of the Laramie Range exhibit cumulus textures and contain trace element abundances which are explained by the accumulation of large volumes of plagioclase. The inverse correlation of Th and La with Sr and the positive correlation of Sc with La in whole-rock samples (discussed above) indicate the presence of trapped in-

Table 4. Data on mineral separates: Laramie Range plagioclase (P), apatite (AP), and magnetite (M). Minerals were separated from whole-rock splits of anorthosite (LRA3, LRA4, LRA5, LRA14), oxide-rich gabbroic anorthosite (LRA13C), and magnetite ore (LRA6, LRA18)

	LRA3P	LRA4P	LRA5P	LRA13CP	LRA14P	LRA6AP	LRA18M
Fe	0.68	1.08	0.50	0.88	0.40	2.18	56.6
Sc	0.31	3.63	0.40	0.72	0.09	1.51	14.6
Cr	1.76	6.26		1.05	1.01		750.0
Co	1.47	2.94	1.88	1.77	0.62	16.0	205.0
Hf	0.10	0.39	0.58	0.75			1.30
Th	0.12	0.27	0.76	0.87	0.07	3.78	
Na	3.93	3.65	3.97	4.12	3.81	0.06	
Rb	7.0	11.0	8.0	14.0	5.0	0.09*	
Cs	0.13	0.19	0.16	0.14			
Ba	718.0	699.0	698.0	908.0	647.0		
La	3.83	4.8	8.1	7.2	2.81	292.0	0.32
Ce	7.6	9.5	14.5	12.0	5.3	660.0	
Nd	2.50	4.02		4.2	1.72	386.0	
Sm	0.407	0.753	0.910	0.740	0.201	99.8	0.17
Eu	2.26	2.16	2.45	3.02	1.64	24.3	0.07
Tb	0.04	0.12	0.12	0.11	0.03	13.1	
Yb	0.09	0.33	0.24	0.28	0.08	17.3	
Lu	0.013	0.047	0.029	0.41		2.13	

Fe and Na in wt.%; remainder of data in ppm

* Analysis by isotope dilution mass spectrometry

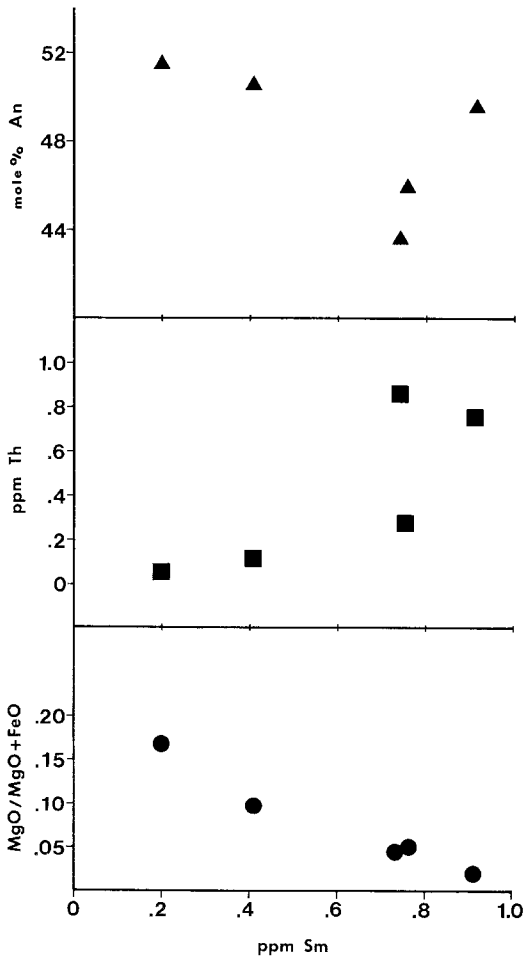

Fig. 8. Plot of ppm Sm versus MgO/MgO + FeO, ppm Th, and mole % An in plagioclase from Laramie Range anorthositic rocks

tercumulus liquid. Large variations in the abundances of REE in plagioclase apparently result from the continued growth of cumulus plagioclase from varying proportions of trapped liquid.

Estimates of the volume of trapped liquid in anorthositic rocks were obtained from a mass balance equation as described by Salpas et al. (1983) using Sc and La abundances in whole-rock and plagioclase mineral separates. Calculated values ranged from 1–6% in anorthosite to 33% trapped liquid in an oxide-rich gabbroic anorthosite (LRA13C). Using an additional mass balance equation similar to the one described by Paster et al. (1974) for cumulus rocks containing trapped liquid, REE abundances in the parental liquid were calculated. Estimated liquids (Fig. 10) are light REE enriched, having an average La_N/Sm_N ratio of 2.2 and La contents ranging from 81 to 159 times chondrites.

Gabbro

Samples of Laramie Range gabbro are fine-grained, iron-rich rocks containing between 10.60 and 42.69 wt.% FeO, and exhibit nearly flat light REE patterns (Figs. 5 and 7). As such, they are texturally and compositionally distinct from anorthositic rocks. Plots of La versus Sr abundances from gabbros and anorthositic rocks exhibit two different trends (Fig. 2), and indicate that gabbros are not mixtures of the cumulus and liquid components which produced anorthositic rocks.

With increasing total REE contents, Laramie Range gabbros exhibit increasing contents of Fe, Sc, Hf, and Zr, decreasing MgO and Sr contents and decreasing Eu_N/Sm_N ratios. These chemical characteristics are consistent with formation of gabbros by either accumulation of increasing proportions of ferromagnesian phases in a parental liquid,

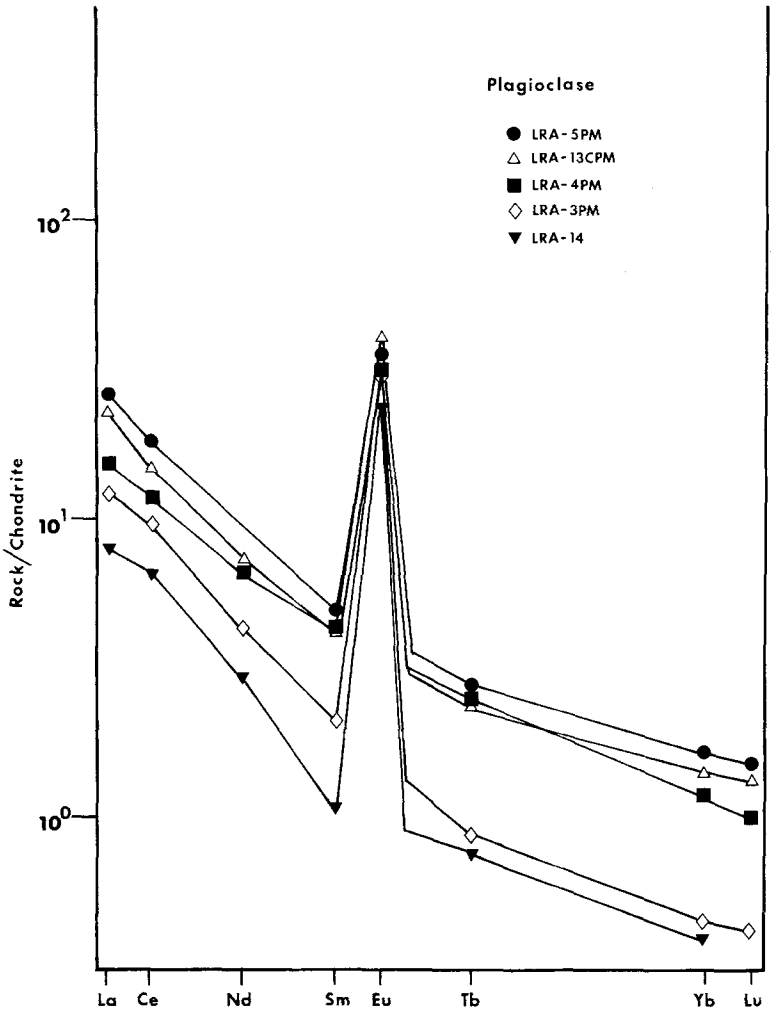

Fig. 9. REE plots of plagioclase mineral separates from Laramie Range anorthositic rocks

Table 5. Representative electron microprobe analyses of plagioclase (P), olivine (OL), and clinopyroxene (PX)

	4-5P	5-4P	8-1P	13C-2P	13D-1P	13E-3P	14-1P
SiO_2	56.30	55.89	56.42	57.70	53.79	54.04	55.88
TiO_2	0.05	0.12	0.10	0.08	0.07	0.11	0.05
Al_2O_3	27.36	27.94	27.11	27.03	30.05	29.80	28.59
FeO	0.19	0.51	0.30	0.22	0.12	0.14	0.15
MgO	0.01	0.01	0.00	0.01	0.00	0.00	0.03
CaO	9.70	10.55	9.71	8.87	11.97	11.24	10.31
Na_2O	5.86	5.70	5.71	6.13	4.41	4.88	5.27
K_2O	0.69	0.35	0.60	0.37	0.35	0.10	0.17
Total	100.16	101.07	99.95	100.41	100.76	100.31	100.45
	1-2OL	8-4OL	13C-1OL	13D-2OL	14-3OL	1-1PX	14-6PX
SiO_2	34.19	33.53	33.93	36.44	36.25	50.42	50.89
TiO_2	0.05	0.08	0.06	0.04	0.05	0.53	1.00
Al_2O_3	0.30	0.42	0.15	0.18	0.21	2.09	4.00
FeO	49.78	47.62	49.51	36.51	40.33	17.95	9.87
MnO	0.77	0.63	0.62	0.42	0.41	0.43	0.25
MgO	16.85	17.95	18.48	28.64	23.20	11.97	13.09
CaO	0.25	0.31	0.06	0.00	0.05	16.56	20.26
Na_2O	0.05	0.02	0.01	0.00	0.01	0.31	0.45
K_2O	0.09	0.04	0.05	0.02	0.04	0.04	0.01
Cr_2O_3	0.07	0.07	0.07	0.04	0.04	0.06	0.07
Total	100.40	100.67	102.96	102.29	100.58	100.36	99.89

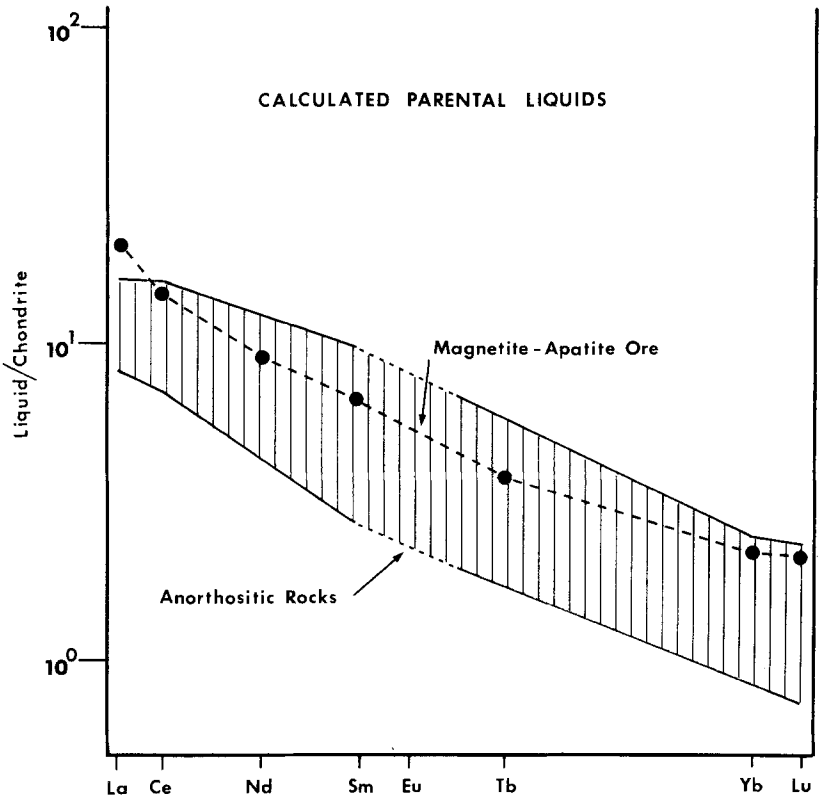

Fig. 10. REE patterns for calculated parental liquids of Laramie Range anorthositic rocks (vertical hatched field) and magnetite-apatite ore (dashed pattern)

Table 6. Sr isotopic data: measured $^{87}Sr/^{86}Sr$ ratios in apatite mineral separates from iron ore, and in whole-rock samples of anorthosite

	$^{87}Sr/^{86}Sr$
Apatite	
LRA6	0.70530
LRA17	0.70537
LRA18	0.70538
LRC1	0.70535
Anorthosite	
LRA5	0.70560
LRA13D	0.70548

or differentiation of a liquid which fractionates plagioclase. The fine-grained appearance and lack of cumulus textures in gabbros indicate that they are not accumulations of ferromagnesian phases. Because gabbros generally have larger MgO/MgO+FeO ratios than those of anorthositic rocks, gabbros are not likely to be late-stage differentiation products of a magma which previously crystallized large volumes of anorthositic rock.

However, plagioclase fractionation is a reasonable explanation for the chemical variations in gabbros if the rocks are early crystallization products of a magma which is parental to anorthositic rocks. According to the model of Emslie (1978), if an olivine tholeiitic magma fractionates pyroxene and minor olivine to produce a high-Al gabbroic magma, and if this high-Al magma crystallizes plagioclase which subsequently accumulates within the crust, then a mechanism is found for producing anorthosite and spatially associated gabbro. Fractionation of minor amounts of plagioclase and mafic silicates from a high-Al gabbroic magma would result in differentiated, iron-enriched gabbros such as LRA7, LRA9, and LRA16, that are compositionally distinct from their parental liquids. Field relations which show Laramie Range anorthosite to be cross-cut by gabbro (Klugman 1966) might thus be expected if an evolved gabbroic magma later intruded a partly solidified plagioclase mass.

Magnetite ore

Samples of magnetite-apatite ore show less pronounced light REE enrichment ($La_N/Sm_N = 1.75$) than do anorthosites, and on a plot of La_N/Sm_N versus Lu_N (Fig. 7) the two groups form a coherent trend. The lower La_N/Sm_N and Eu_N/Sm_N ratios in the ore suggest the fractionation of large volumes of plagioclase from the residual liquid prior to crystallization of the ore. Calculations using the Rayleigh law indicate that approximately 27% crystallization of plagioclase is needed to decrease the La_N/Sm_N ratio from values in an anorthositic parental liquid ($La_N/Sm_N = 2.2$), to values observed in magnetite-apatite ore.

One aim of a petrogenetic study is to estimate compositions of parental magmas. In the case of the anorthosite series, estimates of liquid compositions obtained from plagioclase data may not be representative of late-stage differentiated liquids which are enriched in iron and phosphorus. Apatite has very large REE distribution coefficient values, and it is suggested that the mineral will be a sink for the prevailing REE composition of the liquid. Although REE partitioning will be governed by the mineral's selectivity, relative depletions or enrichments in the REE pattern for apatite should reflect similar characteristics in the magma. Considerable variations in REE patterns for apatite are

observed (Nagasawa 1970; Puchelt and Emmerman 1976), even among apatites from iron ore deposits (Fleischer 1983).

REE data for a fluorapatite megacryst, separated from iron ore sample LRA-6, are presented in Table 4. The sample exhibits light REE enrichment and has a negative Eu anomaly. REE abundances in apatite clearly control abundances in the whole-rock sample. The apatite data presented in Table 4 are similar, in terms of relative abundances, to those of the Bjerkrem-Sogndal anorthosite massif (Roelandts and Duchesne 1979). REE distribution coefficient values for apatite (Roelandts and Duchesne 1979) have been used to estimate the liquid coexisting with apatite (LRA6A). This estimated liquid composition is plotted in Fig. 10 and is similar to the trapped liquid compositions which comprise various proportions of anorthositic rocks.

REE concentrations in whole-rock and in mineral separates from both anorthosite and iron ore are used in calculations which yield similar estimates for parental liquid compositions. Initial $^{87}Sr/^{86}Sr$ ratios in anorthosite are analogous to those in apatite separated from iron ore, and are further evidence that the two rock types are comagmatic. Silicate-free dikes of iron ore are interpreted as residual liquids that evolved from a melt which crystallized anorthosite. The extreme enrichment in Fe, Ti, and P suggests the presence of late-stage residual liquids, and the presence of cross-cutting dikes is taken as evidence that the liquids were mobile. Expeimental evidence suggests that iron oxide magmas can exist at geologically reasonable temperatures of approximately 800–1,000° C in the presence of phosphorus and carbon (Philpotts 1967; Weidner 1982). The iron ore deposits are envisioned as having formed by consolidation of dense interstitial liquids residing in a meshwork of silicate crystals. Subsequent injection of the iron-rich liquids into surrounding, solidified anorthositic rock resulted in numerous dikes of magnetite-apatite ore.

Summary

Anorthosite and spatially associated iron oxide ore from the Laramie Range, Wyoming, are interpreted as comagmatic rocks based on major and trace element data, Sr isotopic ratios, and field relations. Geochemical and textural relations indicate that anorthositic rocks formed as binary mixtures of trapped liquid and cumulus plagioclase. Variations in chemical compositions in whole-rock samples and in mineral separates from anorthositic rocks provide evidence for the presence of trapped intercumulus liquid.

Trace element and textural characteristics of spatially associated gabbros indicate that they are not mixtures of the liquid and cumulus components which produced anorthositic rocks. Rather, the low MgO/MgO + FeO ratios and low Ni abundances in the gabbros indicate that they are evolved mafic rocks. It is suggested that gabbros are differentiation products of a high-Al gabbroic magma that fractionated plagioclase. Accumulation of this plagioclase led to the formation of the anorthosite massif.

Magnetite-apatite ore is considered to be comagmatic with anorthosite based on similar initial $^{87}Sr/^{86}Sr$ ratios and similar estimated parental liquid abundances of REE. Dikes composed of iron oxide and apatite intrude anorthosite, and are regarded as residual liquid segregation deposits.

Acknowledgements. The author thanks John Longhi for constructive comments on the manuscript. The assistance of B. Ron Frost with sample collection is gratefully acknowledged.

References

Albee AL, Ray L (1970) Correction factors for electron probe microanalysis of silicates, oxides, carbonates, phosphates and sulfates. Anal Chem 42:1408–1414

Ashwal LD, Seifert KE (1980) Rare-earth element geochemistry of anorthosite and related rocks from the Adirondacks, New York, and other massif-type complexes. Bull Geol Soc Am 659–684

Ashwal LD (1982) Mineralogy of mafic and Fe–Ti oxide-rich differentiates of the Marcy anorthosite massif, Adirondacks, New York. Am Mineral 67:14–27

Bateman AM (1951) The formation of late magmatic oxide ores. Econ Geol 46:404–426

Bence AE, Albee AL (1968) Empirical correction factors for the electron microanalysis of silicates and oxides. J Geol 76:382–403

Demaiffe D, Hertogen J (1981) Rare earth element geochemistry and strontium isotopic composition of a massif-type anorthositic-charnockitic body: the Hidra Massif (Rogaland, SW Norway). Geochim Cosmochim Acta 45:1545–1561

Diemer RA (1941) Titaniferous magnetite deposits of the Laramie Range, Wyoming. Geol Surv Wyoming Bull 31:1–23

Drake MJ, Weill DF (1975) The partition of Sr, Ba, Ca, Y, Eu^{2+}, Eu^{3+} and other REE between plagioclase feldspar and magmatic silicate liquid: an experimental study. Geochim Cosmochim Acta 39:689–712

Emslie RF (1978) Anorthosite massifs, rapakivi granites, and late Proterozoic rifting of North America. Precambr Res 7:61–98

Fenton MD, Faure G (1969) The strontium isotope composition of the Laramie Range syenite, Wyoming, and its bearing on petrogenesis. Geol Soc Am Abstr 6:15–16

Fleischer M (1983) Distribution of the lanthanides and yttrium in apatites from iron ores and its bearing on the genesis of ores of the Kiruna type. Econ Geol 78:1007–1010

Fountain JC, Hodge DS, Hills FA (1981) Geochemistry and petrogenesis of the Laramie Anorthosite Complex, Wyoming. Lithos 14:113–132

Fowler KS (1930) The anorthosite area of the Laramie Mountains, Wyoming. Am J Sci 19:305–403

Goles GG (1977) Instrumental methods of neutron activation analysis. In: J Zussman (ed) Physical methods in determinative mineralogy. Academic Press, London, pp 343–369

Gordon GE, Randle K, Goles GG, Corliss JB, Beeson MH, Oxley SS (1968) Instrumental activation analysis of standard rocks with high-resolution gama-ray detectors. Geochim Cosmochim Acta 32:369–396

Griffin WL, Sundvoll B, Kristmannsdottir H (1974) Trace element composition of anorthosite plagioclase. Earth Planet Sci Lett 24:213–223

Hagner AF (1968) The titaniferous magnetite deposit of Iron Mountain, Wyoming. In: JD Ridge (ed) Ore deposits of the United States. Am Inst Mineral Metal Petrol Eng, NY, pp 666–680

Heath SA, Fairbairn HW (1969) Sr^{87}/Sr^{86} ratios in anorthosites and associated rocks. In: YW Isachsen (ed) Origin of anorthosite and related rocks. NY State Mus Sci Serv Mem 18:99–110

Hills FA, Armstrong RL (1974) Geochronology of Precambrian rocks in the Laramie Range and implications for the tectonic framework of Precambrian southern Wyoming. Precambr Res 1:213–225

Hills FA, Houston RS (1979) Early proterozoic tectonics of the central Rocky Mountains, North America. Contrib Geol Univ Wyoming 17:89–109

Hodge DS, Owen LB, Smithson SB (1973) Gravity interpretation

of the Laramie anorthosite complex. Wyoming. Bull Geol Soc Am 84:1451–1464
Klugman MA (1966) Resume of the geology of the Laramie anorthosite mass. Mtn Geol 3:75–84
Lister GF (1966) The composition and origin of selected iron-titanium deposits. Econ Geol 61:275–310
Longhi J (1982) Effects of fractional crystallization and cumulus processes on mineral composition trends of some lunar and terrestrial rock series. J Geophys Res 87:A54–A64
Nagasawa H (1970) Rare earth concentrations in zircons and apatites and their host dacites and granites. Earth Planet Sci Lett 9:359–364
Newhouse WH, Hagner AF (1957) Geologic map of anorthosite areas, southern part of the Laramie Range, Wyoming. US Geol Surv Min Inv Field Studies Map MF 119
Norrish K, Chappell BW (1967) X-ray fluorescence spectrography. In: J Zussman (ed) Physical methods in determinative mineralogy. Academic Press, London, pp 161–214
Norrish K, Hutton JT (1969) An accurate X-ray spectrographic method for the analysis of a wide range of geological samples. Geochim Cosmochim Acta 33:431–454
Paster TP, Schauwecker DS, Haskin LA (1974) The behavior of some trace elements during solidification of the Skaergaard layered series. Geochim Cosmochim Acta 38:1549–1577
Philpotts AR (1967) Origin of certain iron-titanium oxide and apatite rocks. Econ Geol 62:303–315
Philpotts AR (1981) A model for the origin of massif-type anorthosites. Can Mineral 19:233–253
Puchelt H, Emmermann R (1976) Bearing of rare earth patterns of apatites from igneous and metamorphic rocks. Earth Planet Sci Lett 31:279–286
Ramberg H (1948) Titanic iron ore formed by dissociation of silicates in granulite facies. Econ Geol 43:553–570
Raedeke LD, McCallum IS (1980) A comparison of fractionation trends in the lunar crust and the Stillwater Complex. Proc Conf Lunar Highlands Crust, Pergamon Press, NY, pp 133–153
Roelandts I, Duchesne JC (1979) Rare-earth elements in apatite from layered norites and iron-titanium oxide ore bodies related to anorthosites (Rogaland, SW Norway). Phys Chem Earth 11:199–212
Ross CS (1941) Occurrence and origin of the titanium deposits of Nelson and Amherst Counties, Virginia. US Geol Surv Prof Pap 198
Salpas PA, Haskin LA, McCallum IS (1983) Stillwater anorthosites: a lunar analog? J Geophys Res 88:B27–B39
Seifert KE (1978) Anorthosite-mangerite relations on Baker Mountain, New York. Bull Geol Soc Am 89:245–250
Simmons EC, Hanson GN (1978) Geochemistry and origin of massif type anorthosites. Contrib Mineral Petrol 66:119–135
Smithson SB, Hodge DS (1972) Field relations and gravity interpretation in the Laramie anorthosite complex. Contrib Geol Univ Wyoming 11:43–59
Subbarayudu GV, Hills FA, Zartman RE (1975) Age and Sr isotopic evidence for the origin of the Laramie anorthosite-syenite complex. Laramie Range, Wyoming. Geol Soc Am Abstr 7:1287
Weidner JR (1982) Iron-oxide magmas in the system Fe–C–O. Can Mineral 20:555–566
Wiebe RA (1980) Anorthosite magmas and the origin of Proterozoic anorthosite massifs. Nature 286:564–567

Received February 2, 1984; Accepted June 11, 1984